scientific reports

Check for updates

OPEN

Elucidating molecular lipid perturbations in trigeminal neuralgia using cerebrospinal fluid lipidomics

Dongyuan Xu[1,3], Xuan Dai[1,3], Qianwen He[2], Zhimin Mei[1], Yixuan Zhou[1], Jingwei Zhao[1] & Nanxiang Xiong[1]✉

Trigeminal neuralgia (TN) is a neuropathic facial pain disorder characterized by severe stabbing pain along the trigeminal nerve. While its pathogenesis remains unclear, nerve demyelination and inflammation are likely involved. Current research has primarily focused on various blood-based omics approaches, which do not fully capture the lipid alterations occurring during TN progression in brain. In contrast, our study is the first to investigate cerebrospinal fluid (CSF) lipidomic profiles in TN patients, aiming to elucidate potential disease mechanisms. CSF samples were collected from 22 TN patients and 18 healthy controls, followed by untargeted lipidomic analysis using high-performance liquid chromatography coupled to quadrupole time-of-flight mass spectrometry. A pipeline for lipid identification and relative quantification, combined with statistical analysis, revealed 188 lipid species across 21 classes. We found significant upregulation of Cer-NPs, LPCs, PCs, TGs, and OxTGs in TN patients, while stigmasterol hexoside was downregulated. Moderate correlations were observed between lipid species and clinical parameters. These findings highlight considerable CSF lipidome alterations in TN, suggesting roles for nerve demyelination, neuroinflammation, and pain sensitization in its pathogenesis. Our study provides novel insights into lipid targets that may offer therapeutic potential for managing TN.

Keywords Trigeminal neuralgia, Cerebrospinal fluid, Lipidomics, Mass spectrometry, Neuroinflammation, Demyelination

Chronic facial pain syndrome known as trigeminal neuralgia (TN) manifests as intermittent, intense, and short-lived episodes of unilateral discomfort and profoundly impacts the quality of life of those afflicted, elevating their susceptibility to depression[1]. These sensations typically occur within the anatomical regions innervated by one or multiple divisions of the fifth cranial nerve (CNV). Epidemiological data reveals a gender disparity in trigeminal neuralgia incidence, with a female predominance, and demonstrates a positive correlation between age and disease onset probability[2]. The genesis of TN is frequently ascribed to neurovascular conflict (NVC) or, alternatively, to tumor-induced compression in the cerebellopontine angle region. These factors are postulated to cause demyelination and subsequent injury to the CNV[3]. Yet, it's noteworthy that NVC is discernible in roughly 17% of CNVs deemed healthy, and strikingly, about 10% of TN patients exhibit no evidence of nerve compression[4]. These findings intimated that the pathogenesis of TN in a significant number of cases is influenced by factors beyond mechanical compression, underscoring the need for a broader understanding of the disease's etiological landscape.

Cerebrospinal fluid (CSF), a transparent and colorless liquid enveloping the central nervous system, serves as a crucial repository for bioactive lipids that partake in myriad physiological functions within the brain and spinal cord[5]. Omics approaches of CSF have played a crucial role in analyzing the etiology of TN, particularly in elucidating signal transduction pathways and demyelination processes. In previous studies, Ericson et al.[6] have employed proteomics to gauge the concentrations of 92 proteins within the CSF. Taking it a step further, Abu Hamdeh et al.[7] utilized TMT-based quantitative proteomics to identify 2552 distinct proteins, with 46 exhibiting significant differential expression compared to controls. Yet, proteomic analysis alone cannot fully elucidate

[1]Department of Neurosurgery, Zhongnan Hospital of Wuhan University, No. 169, Donghu Road, Wuhan 430071, China. [2]Department of Anesthesiology, Zhongnan Hospital of Wuhan University, Wuhan 430071, P. R. China. [3]Dongyuan Xu and Xuan Dai contributed equally to this work. ✉email: mozhuoxiong@163.com

the lipid-mediated processes in TN pathogenesis, including membrane dynamics, lipid-protein interactions, and lipid-dependent signaling cascades. To fill this gap, lipidomics stands as an efficacious analytical approach for the exhaustive characterization of diverse lipids in CSF, enabling the detection and quantification of diverse lipid entities[8]. The application of lipidomics has yielded significant breakthroughs in our understanding of the molecular basis and pathophysiology of various neurological disorders[9–11]. Despite these advances, there is a notable absence of lipidomic data for TN, leaving a significant gap in our understanding of its underlying pathophysiology. This lack of information hinders our ability to fully elucidate the etiology of TN and develop targeted therapeutic strategies.

In this study, we utilized a high-performance liquid chromatography-mass spectrometry (HPLC-MS)-based untargeted lipidomics approach to identify CSF lipidome alterations in TN patients compared to healthy controls. First, we developed and refined protocols for sample preparation and optimized the LC-MS analytical parameters specifically for CSF lipidomics. Subsequently, we performed a quantitative analysis of CSF lipidome in TN patients compared to healthy controls. Finally, we investigated the differentially expressed lipid molecules in TN patients' CSF and conducted correlation analyses with patients' clinical biochemical data. This work illuminated potential lipid-centric mechanisms entangled in the onset and evolution of this condition, thereby enriching our understanding and potentially guiding future therapeutic strategies.

Materials and methods

Reagents and materials

HPLC – grade methanol, dichloromethane, isopropanol, chloroform, acetonitrile, formic acid, and acetic acid were sourced from CNW (ANPEL, Shanghai, China). The reference compounds for internal standardization were procured from Avanti Polar Lipids (Alabaster, AL, USA). The information on all internal standards (ISs) components of Avanti products is listed in Table S1. Sigma-Aldrich (Dorset, UK) provided the deuterated palmitic acid (d4-C16:0). A composite solution comprising all IS was formulated using methanol and preserved at -20 °C for subsequent application. The 14 ISs were each present at 100 μg/mL in this mixture.

Participant description

All samples included in the study were collected in Zhongnan Hospital of Wuhan University, China. This study was approved by the Medical Ethics Committee of Zhongnan Hospital of Wuhan University, China (Grant Number 2022017 K). All participants accepted the goals of the research and signed informed consent prior to the study enrollment. All relevant procedures have been performed in accordance with the Declaration of Helsinki.

This study included 40 subjects: 22 TN patients, and 18 control groups. The entirety of the TN patient cohort satisfied the diagnostic requirements for TN as outlined in the preliminary iteration of the International Classification of Healthcare Disorders' third edition. The control group was composed of patients without nervous system disease. The control group underwent routine surgery for mild colorectal diseases under spinal anesthesia.

CSF sample collection

After being examined and evaluated by a neurosurgeon, all TN patients received MVD surgery for treatment. To obtain surgical space during the operation, some CSF needed to be released after cutting off the dura mater, and this part of CSF was retained for research. MVD and CSF collection were performed by the same neurosurgeon. Lumbar CSF was taken from the control group during lumbar puncture for spinal anesthesia. Lumbar puncture anesthesia and CSF collection are completed by the same anesthetist. CSF specimens should be gathered in aseptic centrifugation vessels and maintained on ice before centrifugal separation. The centrifugation protocol involves subjecting the samples to 2000 times gravitational force at 4 °C for 10 min, thereafter quickly frozen, and stored at – 80 °C.

Lipid extraction

Sample processing referred to the improved Folch method[12]. The protocol involved defrosting all specimens at a temperature of 4 °C. Following this, a 100 μL portion of each specimen was transferred via micropipette into a centrifuge tube with a total capacity of 1.5 mL. Subsequent to the aliquot transfer, each vessel received 1500 μL of a CH_2Cl_2/MeOH (2:1, v/v) along with 10 μL of lipid IS solution. The contents were then subjected to vortex agitation for 10 min. Another 300 μL of 5% acetic acid water was added, vortexed for 30 min, and centrifuged to collect the lower phase. The solvent was evaporated from the extract with nitrogen, and then the residue was reconstituted with 150 μL CH_2Cl_2/IPA (1:1, v/v). To assess analytical result fluctuations from the pooled mixtures and contrast these with instrument-induced errors, a 20 μL portion of each specimen was extracted to serve as quality control (QC) samples. The remaining volume of the specimens underwent analysis via HPLC-MS.

Quality assurance

For continuous assessment of the QTOF6600 system's stability and data quality evaluation, a composite QC sample was formulated by combining equal portions of all individual CSF samples. The data quality was verified using these QC samples, which were introduced into the analytical sequence after every tenth specimen, with a blank sample subsequently injected. This pattern was maintained throughout the entire analytical run.

Untargeted lipidomic analysis based on LC-MS

Lipid profiling was conducted using a chromatography system (Shimadzu 30 A) equipped with an automated sample injection unit (SIL-30 A), featuring a SIL-30 A autosampler. The analytical system employed a reversed-phase column (C18, 100 mm length, 2.1 mm internal diameter, 2.6 μm particle size) coupled with a matching

Phenomenex guard cartridge to enhance column longevity. This setup was interfaced with a quadrupole time-of-flight mass spectrometer (Triple TOF 6600) which was manufactured by Applied Biosystems/MDS Sciex (Concord, ON, Canada) and equipped with electrospray ionization (ESI) source, adapting a previously described methodology[13]. Data collection for both chromatographic separation and mass spectrometric analysis was controlled via Analyst 1.6 (Applied Biosystems). The protocol employed injection volumes of 2 µL and 4 µL for positive and negative ESI modes, respectively. For both ionization analyses, the analytical column was thermostated to maintain a constant temperature of 55 °C during the separation process. A flow rate of 400 µL/min was utilized. The mobile phases consisted of: a 1:1:1 (v: v:v) mixture of water, MeOH, and ACN, supplemented with 5 mM ammonium acetate; a 5:1 (v: v) mixture of IPA and ACN, also containing 5 mM ammonium acetate. The mobile phase composition evolved over time according to the following protocol: (1) Initiation phase (0–0.5 min): Solvent ratio fixed at 4:1 (A: B); (2) First transition (0.5–1.5 min): A: B ratio altered from 4:1 to 3:2; (2) Second transition (1.5–3 min): Further adjustment of A: B from 3:2 to 2:3; (3) Main gradient (3–13 min): Progressive change from 2:3 to 1:49 (A: B); (4) Rapid reset (13–13.1 min): Swift return to initial 4:1 (A: B) ratio; (5) Equilibration (13.1–17 min): Maintenance of 4:1 (A: B) ratio.

Mass spectrometric measurements and fragmentation studies were performed using a data-dependent approach in ESI + and ESI- modes. The MS parameters were configured as follows:

For positive ionization: (1) Declustering potential: 80 V; (2) Collision energy: 35 V; (3) Ion spray voltage: +5500 V; (4) Mass range: 50-1200 *m/z*; (5) Ion source gas 1 and 2: 50 psi each; (6) Curtain gas: 35 psi; (7) Interface heater temperature: 600 °C. For negative ionization: (1) Declustering potential: -80 V; (2) Collision energy: -35 V; (3) Ion spray voltage: -4500 V; (4) Mass range: 50-1200 *m/z*. The gas settings and interface heater temperature for negative mode were maintained identical to those in positive mode.

Identification and relative quantification of lipid compounds

Lipid identification relied on the integration of precise mass measurements, chromatographic retention times (RT), and characteristic MS/MS fragmentation profiles. Raw MS data was processed to detect and align peaks across samples. Lipid profiling was accomplished using a combination of open-source and proprietary software tools. MS-DIAL (version 4.70) platform was utilized alongside commercial applications from SCIEX, including PeakView, MasterView, and MultiQuant. Prior to processing with MS-DIAL, the MS data, initially recorded in SCIEX's proprietary format, underwent conversion to the Analysis Base File format. Lipid identification was performed by MS-DIAL software through a comparison of each feature's MS/MS spectrum against an integrated LipidBlast database[14]. The identification process employed the following criteria: (1) Mass accuracy requirements of less than 0.01 Da for precursor ions and below 0.05 Da for fragment ions; (2) Isotopic pattern matching with a permitted difference of less than 10%; (3) Mass tolerance thresholds of 0.01, 0.05 Da for MS and MS/MS measurements; (4) An identification score cutoff set at 80%.

Following the identification of lipids, a quantitative methodology was developed using MasterView (version 2.0). This method incorporated lipid nomenclature, RT, and mass-to-charge ratios (m/z). Subsequently, this quantitative approach was applied for a more comprehensive analysis (MultiQuant, version 3.0.3). The measurement process for each identified lipid species was performed relative to selected internal standards. Specifically, the relative concentration of individual species was determined by calculating the ratio between the analyte's chromatographic response and that of its corresponding IS.

In the approach to lipid annotation, we utilized established classification systems to designate lipid classes and species. The sum formula notation for lipids adheres to a specific format. This format initiates with an abbreviation indicating the lipid class, followed by two distinct chain descriptions. The first description provides a cumulative tally of carbon atoms and double bonds across all chains. The second description offers a detailed breakdown of individual chains. The two forms are separated by ";", e.g. "PC 34:1; 16:0_18:1".

Statistical analysis

Data presentation employed the format of arithmetic mean accompanied by standard deviation (SD). The entirety of the data collection procedures was executed using Analyst 1.5 software. For subsequent analysis, the original mass concentration data was filled with missing values using the KNN method, and then the Z-Score method was used for data normalization. After normalization, the complex dataset underwent a process of dimensionality reduction to enable clear visualization of metabolic clustering patterns among different sample groups. This was accomplished through the application of multivariate data analysis techniques. The approach incorporated both unsupervised and supervised methods. The unsupervised technique employed was principal components analysis (PCA), which allows for unbiased pattern recognition. In addition, we enhanced our data interpretation via orthogonal partial least-squares discriminant analysis (OPLS-DA). This supervised approach enhances the separation between predefined groups, facilitating the identification of distinguishing features. To control the probability of the first type of error in multiple hypothesis testing, an adjusted *p*-value (*p.adj*) was calculated for nonparametric test (Mann-Whitney U test) in univariate statistical analyses. For meaningful biological interpretation of lipid alterations, we consulted several comprehensive databases. These resources included the LIPID MAPS repository, the Human Metabolome database, and the KEGG database. The nomenclature for the lipid class follows the definition of LIPID MAPS[15]. The lipidomes annotated were subjected to further statistical analysis using software including R studio and SPSS. PCA and OPLSDA are used to observe the clustering situation of quality control samples and the clustering trends of multidimensional data. Select potential bioactive metabolites with $p.adj < 0.05$ and fold change > 2. The concentration difference of lipids from various main classes and subclasses between control and TN groups was calculated (t-test). The screened differential metabolites were combined with clinical biochemical test results for correlation analysis (Spearman analysis).

Results and discussion

Participant description

Demographic characteristics and medical data of the study cohort are summarized in Table 1. The TN group comprised 22 individuals with average age of 55.7 years (SD = 9.5). In comparison, the controls consisted of 18 individuals with average age of 48.1 years (SD = 14.3). Statistical analysis of age distribution between the cohorts, conducted via t-test, revealed no significant disparity ($p = 0.06$). Furthermore, analysis of clinical characteristics revealed no significant disparities between the TN cohort and controls.

Quality control results

To assess and ensure the reliability, reproducibility, and stability of the analytical method, four QC samples were interspersed throughout the analysis. Empirical cumulative distribution curves based on coefficient of variation showed more than 80% of the lipids in QC samples had RSD < 20%. PCA plot displayed the aggregation of quality control samples was good, indicating good instrument stability during the analysis process (Fig. 1).

CSF untargeted lipidomics

A total of 188 lipid compounds from twenty one lipid classes were detected in CSF, including 11 free fatty acids (FFAs), 11 ceramide non-hydroxyfatty acid-sphingosines (Cer-NPs), 10 ceramide alpha-hydroxy fatty acid-sphingosines (Cer-APs), 2 Hexosylceramide alpha-hydroxy fatty acid-sphingosines (HexCer-APs), 3 hexosylceramide hydroxyfatty acid-sphingosines (HexCer-HSs), 2 ceramide hydroxy fatty acid-dihydrosphingosines (Cer-HDSs), 1 ceramide hydroxy fatty acid-sphingosine (Cer-HS), 11 ceramide non-hydroxyfatty acid-sphingosines (Cer-NSs), 11 sphingomyelins (SMs), 2 monogalactosyldiacylglycerols (MGDG), 4 lysophophatidylcholines (LPCs), 12 phosphatidylcholines (PCs), 7 phosphatidylethanolamines (PEs), 15 ether-linked phosphatidylethanolamines (EtherPEs), 4 monoacylglycerols (MGs), 19 diacylglycerols (DGs), 45 triacylglycerols (TGs), 4 oxidized triglycerides (OxTGs), 3 stigmasterol hexosides (SHexs), 6 acylhexosyl sitosterols (AHexSISs), and 5 acylhexosyl stigmasterols (AHexSTSs) (Table S2). Pie chart (Figure S1) showing the composition of the lipidome in CSF. These potential differential compounds were chosen for subsequent analyses, including the concentration difference of 21 subclasses (Table S3) and 12 main classes (Table S4).

Disease-specific lipids

Next, we conducted a multivariate statistical analysis of our lipid profile data. Using OPLSDA for pairwise analysis of the case group and control group, a score plot was drawn, which showed significant separation between the two groups and good predictability (Q2) and fit (R2) were returned through permutation testing, with a $p < 0.05$ value (Fig. 2). Two criteria were used for differential lipids screening, including $p.adj < 0.05$ and VIP > 1, with a fold change > 2. Results for 30 and 23 differential lipids between TN and control groups were obtained, respectively (Fig. 3). Among the identified lipids, 29 showed elevated levels, while 23 exhibited increased expression. Conversely, a single lipid species displayed reduced abundance in TN patients (Table 2). The abundance patterns of these distinctive lipids across both cohorts are visually represented in (Figure S2).

Variable	Control, $N = 18$	TN patients, $N = 22$
Age (y)	48.1 ± 14.3	55.7 ± 9.5
Sex (male/female)	11/7	8/14
Body mass index	23.5 ± 4.0	24.1 ± 2.7
Tobacco use	6	7
Alcohol use	5	7
ASA I	7	10
ASA II	11	12
ASA III	0	0
Hypertension	8	13
Diabetes	0	2
Cardiovascular disease	4	4
IHD	0	0
Stroke	1	0
Peripheral	0	0
Cancer	0	0
Pain (other than TN)	2	4
Fibromyalgia	0	1
Osteoarthritis	0	2
Low back pain	2	0
Rheumatoid arthritis	0	1

Table 1. Participant demographics and clinical profiles: a comparison between TN cases and controls. *ASA* American Society of Anesthesiologists score, *IHD* ischemic heart disease, *N* number of patients, *TN* trigeminal neuralgia.

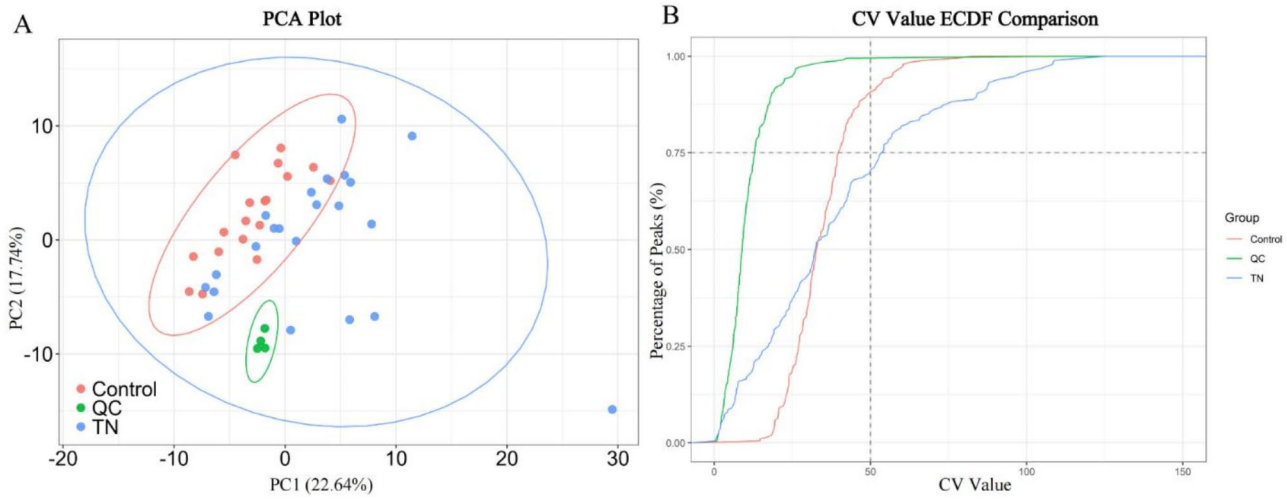

Fig. 1. Sample quality control analysis results. (**A**)The PCA of test and injection QC samples. Individual control and TN samples were considered as test samples, whereas the QC sample was prepared by pooling the test samples. *PCA* principal component analysis, *TN* trigeminal neuralgia. (**B**) Empirical cumulative distribution curves based on CV. *CV* coefficient of variation.

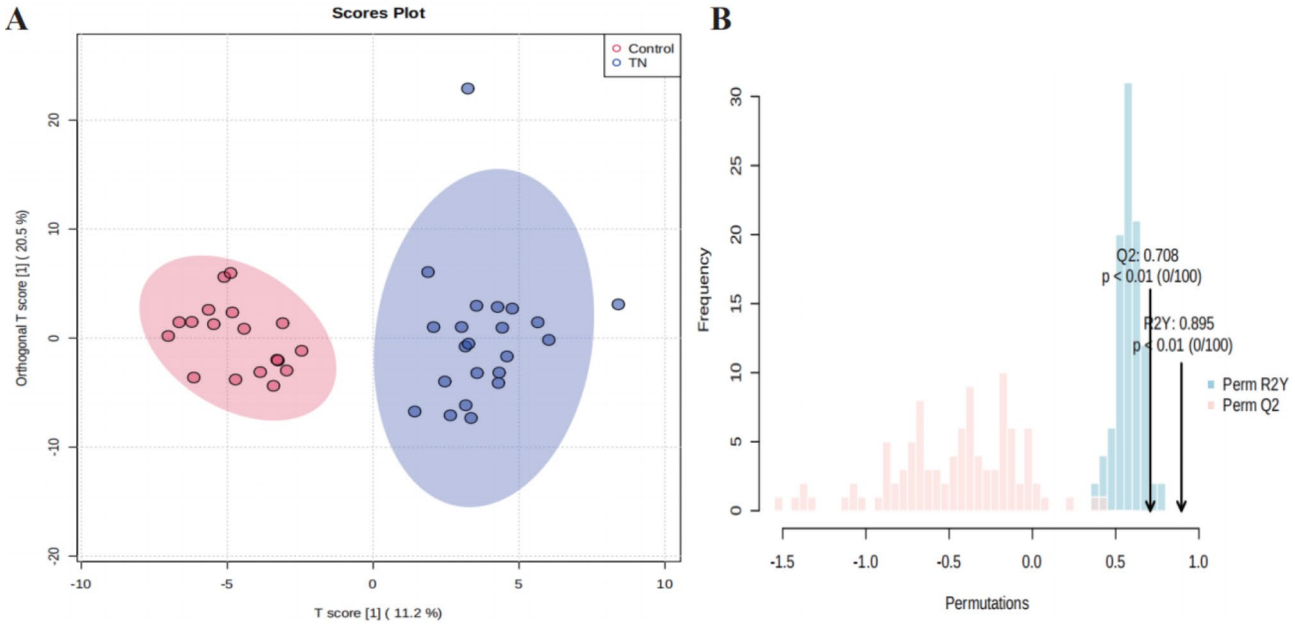

Fig. 2. OPLSDA analysis results. (**A**) OPLSDA score plot of all lipid features in two groups. (**B**) Permutation analysis, showing the observed and cross-validated R_2Y and Q^2 coefficients.

To identify relevant alterations, we further performed a significance analysis of the two groups according to lipid class. To identify relevant alterations, we further conducted a significance analysis (t-test) for the two groups according to lipid class. All detected lipid molecules can be divided into 21 subclasses. 6 lipid subclasses exhibited statistically significant variations between controls and TN, with a threshold of $p < 0.05$, including Cer-NP, PC, LPC, SHex, TG, and OxTG. Except for the concentration of SHex increased in the control group, the others had higher concentrations in the TN group (Fig. 4). The elevated levels of lipid subclasses were quantified as relative abundance ratios between the TN and controls. Of these, the fold increases were detected in PC (2.05), LPC (2.00), Cer-NP (1.68), TG (2.82), and OxTG (1.54), while fold decreases were detected in SHex (0.74) (Table S3). The main class of glycerophosphocholines, including LPC and PC, showed a statistically significant twofold increase compared to controls (from 2.82 ± 0.77 to 5.76 ± 3.47 nmol/CSF mL, $p = 1.15E-03$). In the main class of TG, a nearly threefold increase was detected compared to the controls (from 2.25 ± 0.77 to 6.13 ± 7.27 nmol/CSF mL, $p = 3.01E-02$). Since only SHex was detected in the subclass of sterols, the fold change of sterols is the same as the fold change of SHex (from 7.64 ± 1.74 to 5.69 ± 1.23 nmol/CSF mL, $p = 1.78E-04$). These lipidomic shifts offer

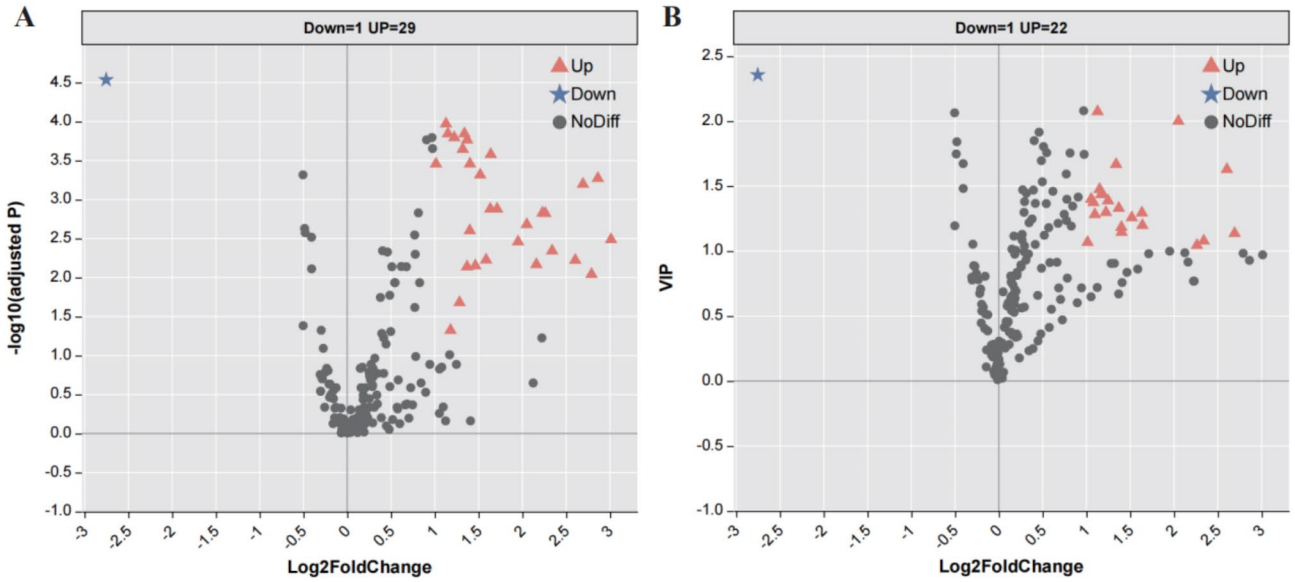

Fig. 3. Volcano plot of differentially expressed lipids. (**A**) Screening of differential lipids was performed using the criterion of adjusted $p < 0.05$ and fold change > 2. Compared to control group, 29 lipids expression were upregulated, while 1 was downregulated in TN group. (**B**) Screening with the criterion of VIP > 1 and fold change > 2. Compared to control group, 22 lipids expression were upregulated, while 1 was downregulated in TN group.

insights into the molecular underpinnings of TN, highlighting a potential link between altered lipid metabolism and the disorder's pathogenesis.

Correlation of clinical data and lipid composition

Subsequently, we analyzed potential associations between clinical data, including age and blood biochemical indicators (liver function, renal function, blood glucose, electrolyte), and CSF lipidomic profiles in TN patients using Spearman's correlation analysis (Fig. 5). Our analysis indicates that lipid concentrations show minimal variation with respect to patient age, as shown in the scatter plot (Figure S3). In liver function-related tests, we found that serum globulin levels were moderately positively correlated with SMs, LPCs, PCs, PEs, and EtherPEs in CSF ($0.4 < r < 0.6$). Alkaline phosphatase and bilirubin were moderately negatively correlated with OxTGs and two kinds of sterol lipids (SHex and AHexSTS) in CSF. In renal function tests, HexCer-AP, DG, and AHexSIS were moderately negatively correlated with cystatin-C and urea, respectively. Electrolyte analysis revealed moderate positive correlations between MG and both chloride and potassium ions, while AHexSIS exhibited a similar relationship specifically with chloride ions. Regarding free radical metabolism, serum superoxide dismutase was moderately positively correlated with HexCer-AP.

These observed correlations intimate a potential intercommunication between lipid metabolic processes and electrolyte homeostasis, as well as antioxidant enzyme activity, within the CSF milieu of TN patients. The intricate relationship between ion channel disturbances and NVC has been the focal point of multiple studies, with particular emphasis on sodium[16] and calcium channels[17]. However, the nexus between other ions and TN remains relatively underexplored. Given these preliminary findings, it becomes imperative to further probe the redox regulation of lipids and the ramifications of alterations in cellular membrane ion flux in the context of TN pathology, to provide a more comprehensive understanding and validation of these observations.

Discussion

TN is a neuropathic disorder characterized by acute, episodic facial pain with an unclear etiology involving demyelination and inflammation. Our lipidomic analysis of CSF in TN patients revealed elevated levels of Cer-NP, PC, LPC, TG, and OxTG, along with reduced stigmasterol hexoside. These findings suggest significant alterations in lipid metabolism associated with TN pathogenesis.

In our study, elevated levels of Cer-NP were observed in the CSF of TN patients, suggesting their potential involvement in neuronal damage and demyelination[18]. Ceramides, including the predominant species Cer 42:2;O3, are known to influence cellular integrity due to their long-chain fatty acids and sphingosine backbone[19,20]. These lipid changes may disrupt myelin structure, a key feature in TN pathophysiology[21]. Additionally, we identified increased levels of FAs such as FA 18:1, FA 16:1, FA 20:0, and FA 24:0, which are associated with membrane fluidity and myelin synthesis[22,23]. These alterations may indicate a response to nerve damage and reflect processes of myelin repair and regeneration in TN[24].

The increased levels of PCs and LPCs observed in our study suggest alterations in cellular membrane composition and fluidity, potentially linked to nerve injury and inflammation[25]. Inflammation is frequently associated with demyelination and has been implicated in the pathogenesis of neuropathic pain in TN. Surgical

Metabolite name	Formula	Adjusted *p*	VIP	Log_2FC
Cer-NP				
Cer 42:2;3O	$C_{42}H_{81}NO_4$	5.98E-03	1.63	2.6
FFA				
FA 16:1	$C_{16}H_{30}O_2$	1.49E-01	1.4	1.05
FA 18:1	$C_{18}H_{34}O_2$	1.41E-01	1.37	1.08
FA 18:2	$C_{18}H_{32}O_2$	9.78E-02	1.44	1.17
FA 18:3	$C_{18}H_{30}O_2$	1.30E-01	1.39	1.25
FA 20:0	C20H40O2	4.57E-01	1.28	1.1
FA 24:0	C24H48O2	4.74E-02	1.44	1.18
LPC				
LPC 16:0	$C_{24}H_{50}NO_7P$	3.49E-04	1.15	1.4
LPC 18:0	$C_{26}H_{54}NO_7P$	4.82E-04	1.26	1.52
PC				
PC 34:1; 16:0_18:1	$C_{42}H_{82}NO_8P$	1.07E-04	2.07	1.13
PC 36:4; 16:0_20:4	$C_{44}H_{80}NO_8P$	1.60E-04	1.3	1.22
PC 38:3; 18:0_20:3	$C_{46}H_{86}NO_8P$	7.27E-03	0.67	1.37
PC 38:4; 18:0_20:4	$C_{46}H_{84}NO_8P$	2.26E-04	0.91	1.32
PC 38:5	$C_{46}H_{82}NO_8P$	3.49E-04	1.07	1.01
PC 38:6; 16:0_22:6	$C_{46}H_{80}NO_8P$	1.72E-04	1.33	1.37
EtherPE				
PE O-36:2; 18:1_18:1	$C_{41}H_{80}NO_7P$	2.91E-05	2.36	-2.75
DG				
DG 32:0; 16:0_16:0	$C_{35}H_{68}O_5$	5.93E-03	0.86	1.59
DG 40:0; 18:0_22:0	$C_{43}H_{84}O_5$	2.09E-03	2	2.05
TG				
TG 48:0; 16:0_16:0_16:0	$C_{51}H_{98}O_6$	1.43E-04	1.48	1.15
TG 48:1; 14:0_16:0_18:1	$C_{51}H_{96}O_6$	1.50E-03	1.04	2.26
TG 48:2; 14:0_16:0_18:2	$C_{51}H_{94}O_6$	3.48E-03	1	1.95
TG 48:3; 12:0_18:1_18:2	$C_{51}H_{92}O_6$	2.50E-03	1.18	1.4
TG 50:1; 16:0_16:0_18:1	$C_{53}H_{100}O_6$	4.54E-03	1.08	2.34
TG 50:3; 16:0_16:1_18:2	$C_{53}H_{96}O_6$	5.34E-04	0.93	2.86
TG 50:4; 14:0_18:2_18:2	$C_{53}H_{94}O_6$	1.32E-03	0.98	1.71
TG 52:1; 16:0_18:0_18:1	$C_{55}H_{104}O_6$	6.34E-04	1.14	2.69
TG 52:2; 16:0_18:1_18:1	$C_{55}H_{102}O_6$	9.08E-03	0.98	2.79
TG 52:3; 16:0_18:1_18:2	$C_{55}H_{100}O_6$	3.25E-03	0.97	3.01
TG 52:4; 16:0_18:2_18:2	$C_{55}H_{98}O_6$	6.79E-03	0.92	2.16
TG 52:5; 16:0_18:2_18:3	$C_{55}H_{96}O_6$	2.09E-02	0.9	1.28
TG 54:1; 18:0_18:0_18:1	$C_{57}H_{108}O_6$	1.32E-03	1.29	1.63
TG 56:6; 18:1_18:2_20:3	$C_{59}H_{102}O_6$	1.48E-03	0.77	2.23
TG 56:7; 16:0_20:3_20:4	$C_{59}H_{100}O_6$	7.05E-03	0.84	1.46
OxTG				
TG 43:2;1O; 10:0_16:0_17:2;1O	$C_{46}H_{84}O_7$	1.43E-04	1.67	1.34
TG 49:3;1O; 16:0_16:0_17:3;1O	$C_{52}H_{94}O_7$	2.64E-04	1.2	1.64

Table 2. Lipids with p.adj < 0.05 or VIP > 1, and fold change > 1. Positive Log2FC values indicate elevated lipid levels, while negative values denote reduced levels.

findings of adhesive inflammatory arachnoid membranes in the NVC area further support the involvement of inflammation in TN[26]. The upregulation of PCs may reflect enhanced synthesis for membrane repair and regeneration[27]. Similarly, LPCs, while often associated with inflammation, may also indicate active membrane turnover and repair processes in TN[28]. The observed increase in DGs, particularly DG.32:0 and DG.40:0, indicates disruptions in lipid synthesis and remodeling, which may impact neural membrane function[29]. Similarly, elevated levels of TG and OxTG suggest broader disturbances in lipid metabolism. Although their precise role in TN is unclear, these changes may reflect underlying metabolic alterations associated with the disease.

Our study identified a significant reduction in PE O-36:2, an ether phospholipid, in the CSF of TN patients. Stigmasterol hexoside, a phytosterol with anti-inflammatory and neuroprotective properties, was also found to

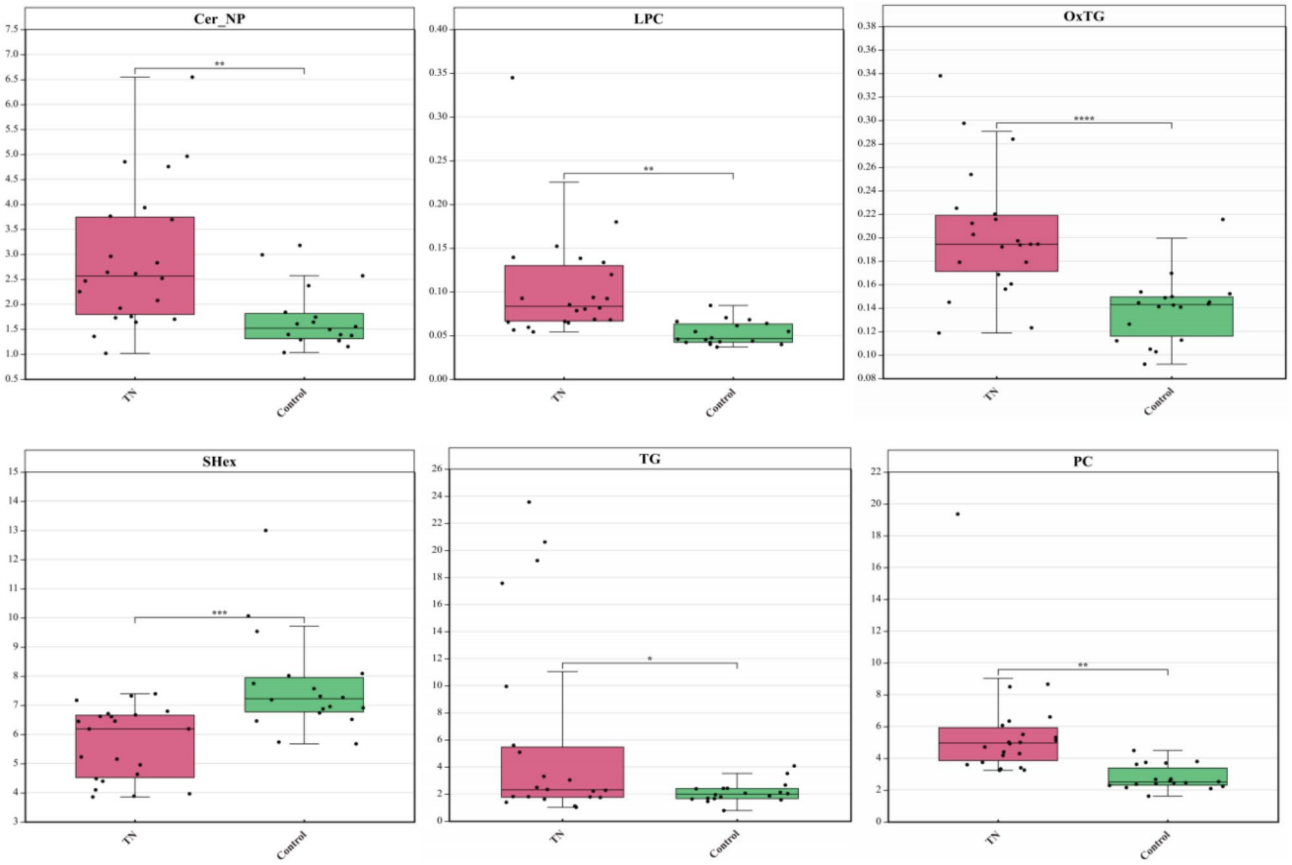

Fig. 4. Significantly different expression of lipid subclasses. Boxplot of six significantly different lipid subclasses, including Cer-NP, LPC, PC, TG, OxTG, and SHex. Except for Shex, the other five have higher average concentrations in the TN group. (*Cer-NP* ceramide non-hydroxyfatty acid-sphingosine, *LPC* lysophosphatidylcholine, *PC* phosphatidylcholine, *TG* triacylglycerol, *OxTG* oxidized triglyceride, *SHex* stigmasterol hexoside. *$p < 0.05$, **$p < 0.01$, ***$p < 0.001$, ****$p < 0.0001$).

be decreased[30]. These reductions may indicate disruptions in lipid homeostasis and a diminished capacity for neuroprotection in TN[31,32]. Further investigation is needed to clarify their roles in the disease.

Conclusion

Untargeted lipidomic analysis of CSF in patients with TN provides valuable insights into the complex lipid alterations associated with this debilitating disorder. The upregulation of ceramides, FAs, PCs, LPCs, DGs, and TGs indicates their potential involvement in nerve demyelination, inflammation, lipid synthesis, and remodeling, shedding light on potential mechanisms underlying TN. Further investigations are warranted to elucidate the functional significance of these lipid changes and their therapeutic implications for managing this challenging condition.

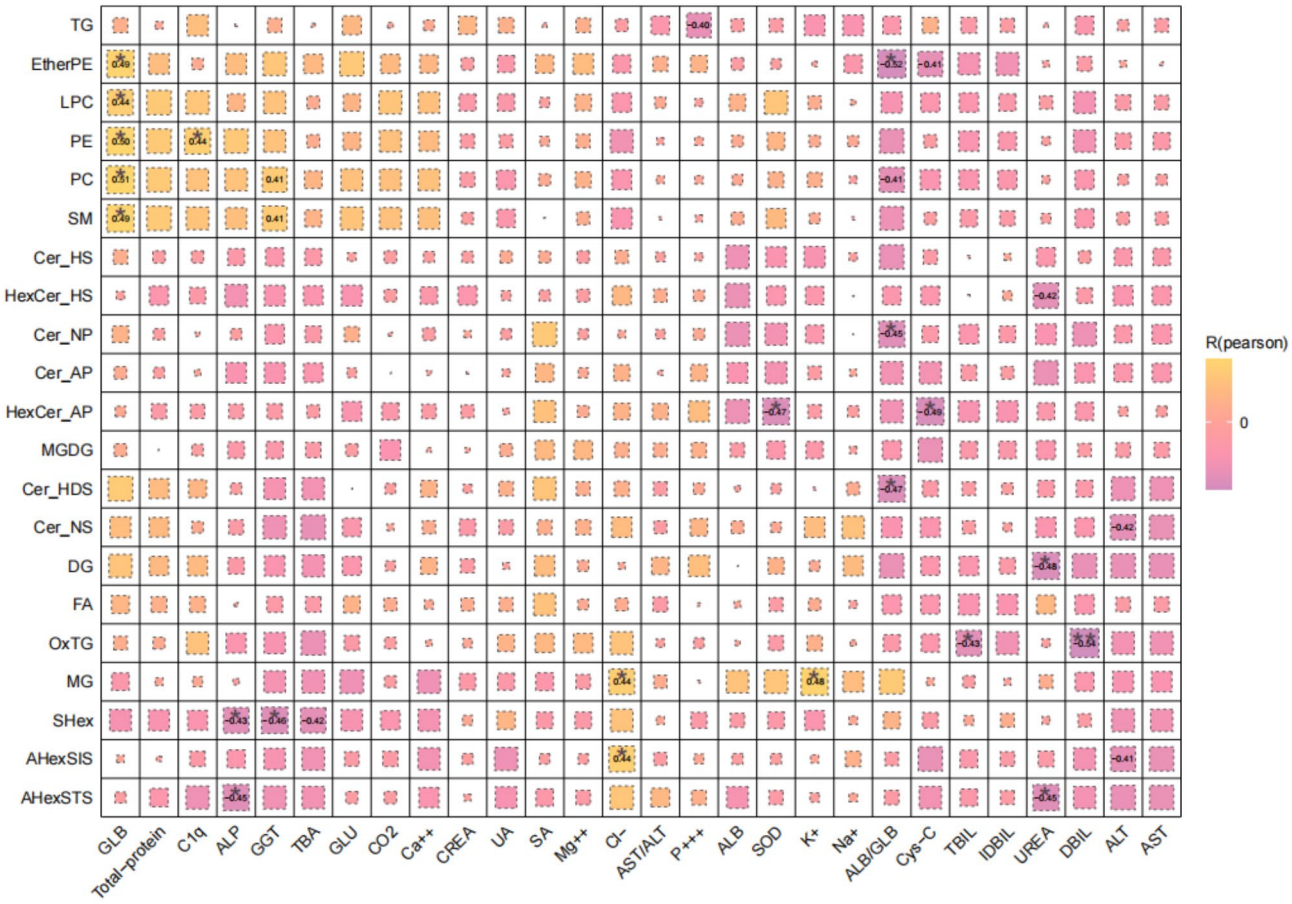

Fig. 5. Correlation analysis between clinical biochemical indexes and lipid expression. Correlation heatmap, showing the Pearson's correlation between laboratory biochemical tests (liver function test, renal function test, blood glucose, and electrolyte) and lipid subclasses in TN patients. *, indicates significance less than 0.05, while a correlation coefficient is shown. *GLB* globulin, *ALP* alkaline phosphatase, *GGT* glutamyl transpeptidase, *TBA* total bile acid, *GLU* glucose, *CREA* creatinine, *UA* uric acid, *SA* serum amyloid protein, *AST* aspartate aminotransferase, *ALT* alanine aminotransferase, *ALB* albumin, *SOD* superoxide dismutase, *Cys-C* cystatin-C, *TBIL* total bilirubin, *IDBIL* indirect bilirubin, *DBIL* direct bilirubin.

Data availability

All data generated or analyzed during this study are included in this published article and its supplementary information files. The datasets generated and analysed during the current study are also available in the MetabolLights repository (MTBLS11086). The lipidomics minimum reporting checklist is available (https://doi.org/10.5281/zenodo.14523180).

Received: 7 September 2024; Accepted: 7 February 2025
Published online: 06 April 2025

References

1. Cruccu, G., Di Stefano, G. & Truini, A. Trigeminal neuralgia. *N. Engl. J. Med.* **383** (8), 754–762. https://doi.org/10.1056/NEJMra1914484 (2020).
2. Mueller, D. et al. Prevalence of trigeminal neuralgia and persistent idiopathic facial pain: a population-based study. *Cephalalgia* **31** (15), 1542–1548. https://doi.org/10.1177/0333102411424619 (2011).
3. Love, S., Hilton, D. A. & Coakham, H. B. Central demyelination of the vth nerve root in trigeminal neuralgia associated with vascular compression. *Brain Pathol.* **8** (1), 1–11. https://doi.org/10.1111/j.1750-3639.1998.tb00126.x (1998). discussion 11 – 2.
4. Antonini, G. et al. Magnetic resonance imaging contribution for diagnosing symptomatic neurovascular contact in classical trigeminal neuralgia: a blinded case-control study and meta-analysis. *Pain* **155** (8), 1464–1471. https://doi.org/10.1016/j.pain.2014.04.020 (2014).
5. Colsch, B., Seyer, A., Boudah, S. & Junot, C. Lipidomic analysis of cerebrospinal fluid by mass spectrometry-based methods. *J. Inherit. Metab. Dis.* **38** (1), 53–64. https://doi.org/10.1007/s10545-014-9798-0 (2015).
6. Ericson, H. et al. Cerebrospinal fluid biomarkers of inflammation in trigeminal neuralgia patients operated with microvascular decompression. *Pain* **160** (11), 2603–2611. https://doi.org/10.1097/j.pain.0000000000001649 (2019).
7. Abu Hamdeh, S. et al. Increased CSF levels of apolipoproteins and complement factors in trigeminal Neuralgia Patients-In depth proteomic analysis using Mass Spectrometry. *J. Pain.* **21** (9–10), 1075–1084. https://doi.org/10.1016/j.jpain.2020.03.002 (2020).

8. Ghosh, A. & Nishtala, K. Biofluid lipidome: a source for potential diagnostic biomarkers. *Clin. Transl. Med.* **6** (1), 22. https://doi.org/10.1186/s40169-017-0152-7 (2017).
9. Wentling, M. et al. A metabolic perspective on CSF-mediated neurodegeneration in multiple sclerosis. *Brain* **142** (9), 2756–2774. https://doi.org/10.1093/brain/awz201 (2019).
10. He, Y. et al. Prosaposin maintains lipid homeostasis in dopamine neurons and counteracts experimental parkinsonism in rodents. *Nat. Commun.* **14** (1), 5804. https://doi.org/10.1038/s41467-023-41539-5 (2023).
11. Qiu, S. et al. Adult-onset CNS myelin sulfatide deficiency is sufficient to cause Alzheimer's disease-like neuroinflammation and cognitive impairment. *Mol. Neurodegener.* **16** (1), 64. https://doi.org/10.1186/s13024-021-00488-7 (2021).
12. Reichl, B. et al. Evaluation and optimization of common lipid extraction methods in cerebrospinal fluid samples. *J. Chromatogr. B.* 1153122271. https://doi.org/10.1016/j.jchromb.2020.122271 (2020).
13. Hu, A. et al. Comprehensive and high-coverage lipidomic analysis of oilseeds based on ultrahigh-performance liquid chromatography coupled with electrospray ionization quadrupole time-of-flight mass spectrometry. *J. Agric. Food Chem.* **69** (32), 8964–8980. https://doi.org/10.1021/acs.jafc.0c07343 (2021).
14. Tsugawa, H. et al. MS-DIAL: data-independent MS/MS deconvolution for comprehensive metabolome analysis. *Nat. Methods.* **12** (6), 523–526. https://doi.org/10.1038/nmeth.3393 (2015).
15. Kind, T. et al. LipidBlast in silico tandem mass spectrometry database for lipid identification. *Nat. Methods.* **10** (8), 755–758. https://doi.org/10.1038/nmeth.2551 (2013).
16. Liu, M. X., Zhong, J., Xia, L., Dou, N. N. & Li, S. T. IL-6 contributes to na(v)1.3 up-regulation in trigeminal nerve following chronic constriction injury. *Neurol. Res.* **42** (6), 504–514. https://doi.org/10.1080/01616412.2020.1747719 (2020).
17. Gualdani, R. et al. Trigeminal neuralgia TRPM8 mutation: enhanced activation, basal [Ca(2+)](i) and menthol response. *Neurol. -Genet.* **7** (1), e550. https://doi.org/10.1212/nxg.0000000000000550 (2021).
18. Zeidan, Y. H. & Hannun, Y. A. Translational aspects of sphingolipid metabolism. *Trends Mol. Med.* **13** (8), 327–336. https://doi.org/10.1016/j.molmed.2007.06.002 (2007).
19. Hannun, Y. A. & Obeid, L. M. Principles of bioactive lipid signalling: lessons from sphingolipids. *Nat. Rev. Mol. Cell. Biol.* **9** (2), 139–150. https://doi.org/10.1038/nrm2329 (2008).
20. Salvemini, D., Doyle, T., Kress, M. & Nicol, G. Therapeutic targeting of the ceramide-to-sphingosine 1-phosphate pathway in pain. *Trends Pharmacol. Sci.* **34** (2), 110–118. https://doi.org/10.1016/j.tips.2012.12.001 (2013).
21. Marinković, S. et al. Ultrastructure and immunohistochemistry of the trigeminal peripheral myelinated axons in patients with neuralgia. *Clin. Neurol. Neurosurg.* **111** (10), 795–800. https://doi.org/10.1016/j.clineuro.2009.07.020 (2009).
22. Rumora, A. E. et al. The divergent roles of dietary saturated and monounsaturated fatty acids on nerve function in murine models of obesity. *J. Neurosci.* **39** (19), 3770–3781. https://doi.org/10.1523/jneurosci.3173-18.2019 (2019).
23. Lei, E., Vacy, K. & Boon, W. C. Fatty acids and their therapeutic potential in neurological disorders. *Neurochem. Int.* **95**, 75–84. https://doi.org/10.1016/j.neuint.2016.02.014 (2016).
24. Poitelon, Y., Kopec, A. M. & Belin, S. Myelin fat facts: an overview of lipids and fatty acid metabolism. *Cells* **9** (4), 812. https://doi.org/10.3390/cells9040812 (2020).
25. Klein, J. Membrane breakdown in acute and chronic neurodegeneration: focus on choline-containing phospholipids. *J. Neural Transm. (Vienna).* **107** (8–9), 1027–1063. https://doi.org/10.1007/s007020070051 (2000).
26. Szmyd, B. et al. The underlying pathogenesis of neurovascular compression syndromes: a systematic review. *Front. Molec. Neurosci.* https://doi.org/10.3389/fnmol.2022.923089 (2022).
27. Walter, A. et al. Glycerophosphocholine is elevated in cerebrospinal fluid of Alzheimer patients. *Neurobiol. Aging.* **25** (10), 1299–1303. https://doi.org/10.1016/j.neurobiolaging.2004.02.016 (2004).
28. Fonteh, A. N., Pogoda, J. M., Chung, R., Cowan, R. P. & Harrington, M. G. Phospholipase C activity increases in cerebrospinal fluid from migraineurs in proportion to the number of comorbid conditions: a case-control study. *J. Headache Pain.* **14** (1), 60. https://doi.org/10.1186/1129-2377-14-60 (2013).
29. Park, K. A. & Vasko, M. R. Lipid mediators of sensitivity in sensory neurons. *Trends Pharmacol. Sci.* **26** (11), 571–577. https://doi.org/10.1016/j.tips.2005.09.010 (2005).
30. Uddin, G. et al. Anti-nociceptive, anti-inflammatory and sedative activities of the extracts and chemical constituents of Diospyros lotus L. *Phytomedicine* **21** (7), 954–959. https://doi.org/10.1016/j.phymed.2014.03.001 (2014).
31. Rubio, J. M., Astudillo, A. M., Casas, J., Balboa, M. A. & Balsinde, J. Regulation of phagocytosis in macrophages by membrane ethanolamine plasmalogens. *Front. Immunol.* **9**, 1723. https://doi.org/10.3389/fimmu.2018.01723 (2018).
32. Jie, F. et al. Stigmasterol attenuates inflammatory response of microglia via NF-κB and NLRP3 signaling by AMPK activation. *Biomed. Pharmacother.* https://doi.org/10.1016/j.biopha.2022.113317 (2022).

Acknowledgements

This work was financially supported by National Key Research and Development Program 329 of China [2022YFB4702805]. The authors thank Xin Lv for technical contributions.

Author contributions

Dongyuan Xu and Xuan Dai wrote the main manuscript text. Dongyuan Xu prepared all the figures and tables. Qianwen He, Zhimin Mei, Yixuan Zhou, and Jingwei Zhao helped collect clinal samples and data. Nanxiang Xiong revised and supervised the manuscript. All authors reviewed the manuscript.

Declarations

Competing interests

The authors declare no competing interests.

Additional information

Supplementary Information The online version contains supplementary material available at https://doi.org/10.1038/s41598-025-89755-x.

Correspondence and requests for materials should be addressed to N.X.